

# Highly efficient cycloreversion of photochromic dithienylethene compounds using visible light-driven photoredox catalysis†

Cite this: *Chem. Sci.*, 2014, 5, 1463Sumin Lee,<sup>a</sup> Youngmin You,<sup>\*b</sup> Kei Ohkubo,<sup>c</sup> Shunichi Fukuzumi<sup>\*ac</sup>  
and Wonwoo Nam<sup>\*a</sup>

Photochromic *cis*-1,2-dithienylethene (DTE) compounds are the most suitable to the application in reversible molecular memories and switches, but imbalance in the quantum yields for the chromic interconversion limits the full potentials. We have demonstrated and investigated photoelectrocatalytic cycloreversion of DTE compounds. A series of cyclometalated Ir(III) complexes served as photoredox catalysts to achieve one order of magnitude enhancement in the cycloreversion quantum yields. The mechanism, involving photoinduced oxidation of DTE, electrocatalytic ring opening and reductive termination, has been thoroughly investigated. Nanosecond transient spectroscopic techniques were employed to directly monitor bidirectional electron transfer between DTE and the photoredox catalyst. It was found that the oxidative photoinduced electron transfer was diffusion-controlled and located in the Marcus-normal region, whereas the competing back electron transfer occurred in the Marcus-inverted region. This novel discovery establishes that synthetic control over back electron transfer, rather than photoinduced electron transfer, can improve the performance of the photoelectrocatalysis. Combined studies, including the kinetic investigations with the use of variable-temperature stopped-flow UV-vis absorption spectroscopy and quantum chemical calculations based on time-dependent density functional theory, further enabled identification of the radical intermediate that underwent thermal, electrocatalytic cycloreversion. Finally, analyses based on the Marcus theory of electron transfer suggested regeneration of the excited-state catalyst in the termination step to initiate dark-state electrocatalytic cycloreversion. The results obtained in this work established novel principles to maximizing quantum yields for photoinduced cycloreversion of DTEs. It is envisioned that our findings will provide novel guidance to the future application of the truly reversible photochromism to a broad range of molecular photonic systems.

Received 19th October 2013  
Accepted 20th December 2013

DOI: 10.1039/c3sc52900b

[www.rsc.org/chemicalscience](http://www.rsc.org/chemicalscience)

<sup>a</sup>Department of Bioinspired Science, Ewha Womans University, Daehyun-dong, Seodaemun-gu, Seoul 120-750, Korea. E-mail: [wynam@ewha.ac.kr](mailto:wynam@ewha.ac.kr) (W. N.)

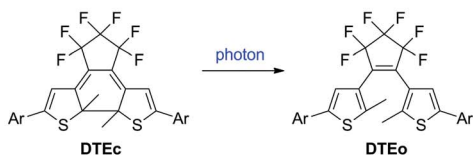
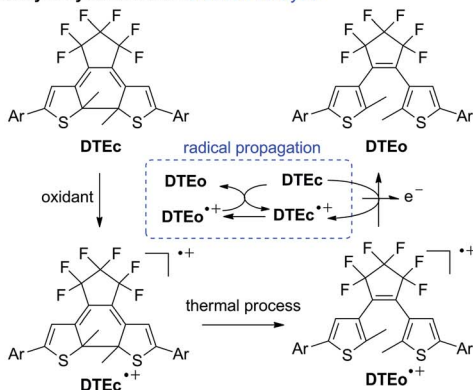
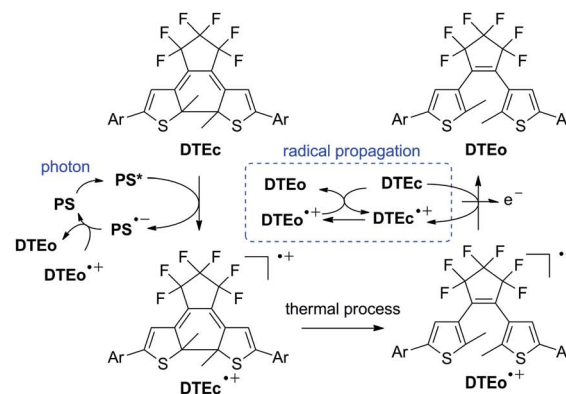
<sup>b</sup>Department of Advanced Materials Engineering for Information and Electronics, Kyung Hee University, Seocheon-dong, Yongin, Gyeonggi-do 446-701, Korea. E-mail: [odds2@khu.ac.kr](mailto:odds2@khu.ac.kr) (Y. Y.)

<sup>c</sup>Department of Material and Life Science, Graduate School of Engineering, Osaka University, ALCA, Japan Science and Technology Agency (JST), Suita, Osaka 565-0871, Japan. E-mail: [fukuzumi@chem.eng.osaka-u.ac.jp](mailto:fukuzumi@chem.eng.osaka-u.ac.jp) (S. F.)

† Electronic supplementary information (ESI) available: Experimental details; Fig. S1–S27, voltammograms and UV-vis absorption spectra of the Ir(III) complexes and the DTE compounds, <sup>1</sup>H NMR spectra showing photoelectrocatalytic cycloreversion of PhDTEc by IrOMe, plots of PCQY<sub>C→O</sub> at various concentrations of IrOMe, plots of PCQY<sub>C→O</sub> vs. the inverse of the phosphorescence lifetimes of the Ir(III) complexes, photoluminescence decay traces and the determination of the rate constants for PeT, laser flash photolysis results and the determination of the rate constants for BeT, plots of PCQY<sub>C→O</sub> vs. the driving force for BeT, plots of log *k*<sub>BeT</sub> vs.  $-\Delta G_{\text{BeT}}$  for PhDTE, MDTE, CDTE and ADTE, variable-temperature stopped-flow UV-vis absorption spectra, delayed photoluminescence of Irppy, and copies of the <sup>1</sup>H, <sup>13</sup>C and <sup>19</sup>F NMR spectra of ADTE and its precursors; Table S1, listing the rate constants for PeT. See DOI: 10.1039/c3sc52900b

## Introduction

*cis*-1,2-Dithienylethene (DTE) compounds display a reversible chromic interconversion between an open form (DTEo) and a closed form (DTEc) under alternating photoirradiation (Scheme 1a).<sup>1,2</sup> The photochromism of DTEs is superior to other molecular photochromism in many aspects, such as bistability, full reversibility, ultrafast conversion rates and extreme fatigue resistance.<sup>3</sup> Photochromic DTE compounds have thus been considered as the ideal candidate for widespread applications, ranging from molecular switches to memories.<sup>4–7</sup> The photonic application, however, has frequently been hampered by low efficiencies of cycloreversion to DTEo. The quantum yields for photochromic cycloreversion (PCQY<sub>C→O</sub>) are typically smaller than the quantum yields for cyclization (PCQY<sub>O→C</sub>) by factors of 10<sup>−2</sup> to 10<sup>−1</sup>. To improve PCQY<sub>C→O</sub>, synthetic controls, including variations in the substituents of the DTE framework,<sup>8</sup> have extensively been explored. The studies have shown that the quantum yields are susceptible to subtle changes in the

(a) Conventional photochromic cycloreversion: *photon-stoichiometric*(b) Electrocatalytic cycloreversion: *electron-catalytic*(c) Photoelectrocatalytic cycloreversion: *photon-catalytic*

Scheme 1 Cycloreversion of DTE compounds: (a) photochromic cycloreversion, (b) electrocatalytic cycloreversion and (c) photoelectrocatalytic cycloreversion.

electronic structure of DTEs.<sup>9–28</sup> Alternative strategies to improving the cycloreversion quantum yield involve utilization of the electronic states with low barriers for chromic interconversion. PCQY<sub>C→O</sub> values as high as 0.5 were achieved by multi-photon excitation<sup>29–31</sup> and triplet sensitization.<sup>32</sup> These demonstrations promise the potential for fully reversible photochromism. Nevertheless, the use of sophisticated instruments and the photophysical conditions for multi-photon processes and triplet–triplet energy transfer remain significant drawbacks.

Many photochromic DTEs undergo cycloreversion upon oxidation, as observed by us<sup>33</sup> and the research groups of Akita,<sup>34,35</sup> Branda,<sup>36–40</sup> Feringa,<sup>41,42</sup> Irie,<sup>43</sup> Kawai,<sup>44,45</sup> and Launay.<sup>46,47</sup> While the oxidative cycloreversion is still the subject of intense research interests, it provides a unique basis to improve cycloreversion quantum yields because the electrochromism is nearly barrierless and electrocatalytic.<sup>48</sup> In particular, the electrocatalytic cycloreversion can produce considerably high net current efficiencies due to the highly exergonic radical propagation, as recently proved by the Kawai group (Scheme 1b).<sup>44</sup> By taking advantage of electrochromism, we previously devised the photoelectrocatalysis strategy and achieved improved cycloreversion quantum yields.<sup>49</sup> The photoinduced cycloreversion was initiated by one-electron oxidation of DTEc by a photoredox catalyst. The combination of photoredox catalysis and a radical chain reaction between DTEc and DTEo provided improved photon economy (Scheme 1c). In addition, this strategy uniquely retained the full merits of photochromism and electrochromism because the ‘photon-mode’ interconversion comprising the photoelectrocatalytic cycloreversion and the photochromic cyclization was fully reversible, as demonstrated by high fatigue resistance upon repeated chromic cycles.

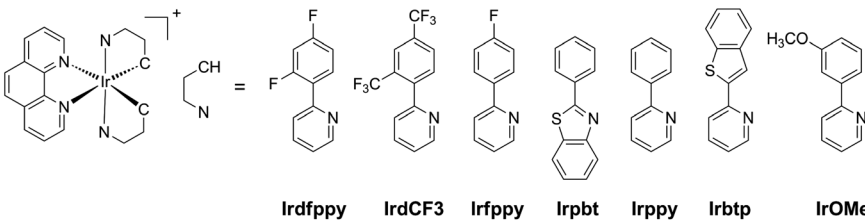
This initial success provided a motivation for investigations into molecular factors affecting the quantum yield for

photoelectrocatalytic cycloreversion (PeCQY<sub>C→O</sub>). Elucidation and control of the factors would ultimately enable highly efficient, reversible molecular photochromism, which would be valuable to a broad range of chromic applications. Moreover, the study would be of great significance, as the mechanism involving photo-generated radical intermediates has strong resemblance to many photoredox catalytic reactions.<sup>50–53</sup> It should be noted that the mechanistic details about the photoelectrocatalytic chromism has not been investigated to date. To this end, we designed mechanistic studies on the photoelectrocatalysis systems employing cyclometalated Ir(III) complexes as visible light-driven photoredox catalysts (see Table 1). The heteroleptic constructs of the complexes with the systemically controlled ligand structures provided a unique opportunity to correlate the molecular parameters and PeCQY<sub>C→O</sub>. Five DTE compounds with varying extents of electron densities were employed (see Table 2). PeCQY<sub>C→O</sub> values for 35 combinations of the photoredox catalysts and DTE compounds were determined by ferrioxalate actinometry. We directly monitored the oxidative photoinduced electron transfer and the reductive back electron transfer by employing time-resolved spectroscopy techniques. Cycloreversion of the radical intermediates was observed by variable-temperature stopped-flow UV-vis absorption spectroscopy. Finally, the termination step to produce DTEo was analyzed on the basis of the Marcus theory of electron transfer.

## Results and discussion

### Quantum yields for photoelectrocatalytic cycloreversion

Chemical structures along with the photophysical and the electrochemical data for the cyclometalated Ir(III) complexes ([Ir<sup>III</sup>(C/N)<sub>2</sub>phen]PF<sub>6</sub>; C/N = cyclometalating ligand, phen = 1,10-phenanthroline) and DTE compounds are shown in Tables 1

Table 1 Photophysical and electrochemical data for the photoredox catalysts<sup>a</sup>


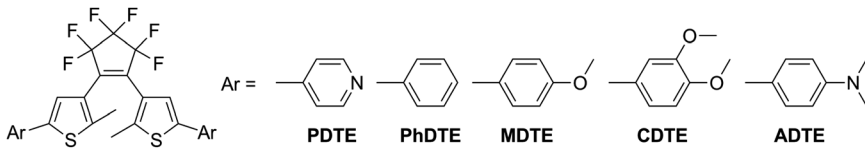
	$\lambda_{\text{abs}}(\text{MLCT})^b/\text{nm}$	$\Delta E_{\text{T}}^c/\text{eV}$	$E_{1/2}(\text{Ir}^{\text{III/IV}})^d$ (vs. SCE)/V	$E_{\text{red}}^e$ (vs. SCE)/V	$E_{\text{red}}^{*f}$ (vs. SCE)/V	$\tau^g/\mu\text{s}$	PLQY <sup>h</sup>	$k_{\text{r}}^i/10^4 \text{ s}^{-1}$	$k_{\text{nr}}^j/10^5 \text{ s}^{-1}$
Irdfppy	410	2.82	1.56	-1.30	1.52	1.79	0.12	6.7	4.9
IrdCF3	410	2.72	1.70	-1.27	1.45	6.25	0.21	3.4	1.3
Irfppy	410	2.70	1.42	-1.34	1.36	1.35	0.17	13	6.1
Irpbt	420	2.58	1.39	-1.31	1.27	4.07	0.14	3.4	2.1
Irppy	410	2.55	1.19	-1.37	1.18	1.26	0.09	7.1	7.1
Irbtp	420	2.44	1.06	-1.28	1.16	2.15	0.10	4.7	4.2
IrOMe	420	2.39	0.94	-1.38	1.01	0.0637	0.0021	3.3	157

<sup>a</sup> Some data were taken from ref. 54. <sup>b</sup> MLCT absorption bands; 10  $\mu\text{M}$  in acetonitrile solutions, 298 K. <sup>c</sup> Triplet state energy determined at the intersection between the UV-vis absorption and the phosphorescence spectra. <sup>d</sup> Ground-state oxidation and <sup>e</sup> ground-state reduction potentials determined by cyclic voltammetry (CV) and differential pulse voltammetry (DPV). *Conditions:* scan rate = 100 and 0.4  $\text{mV s}^{-1}$  for CV and DPV, respectively; 1.0 mM Ir complex in an Ar-saturated acetonitrile containing 0.10 M  $\text{Bu}_4\text{NPF}_6$  supporting electrolyte; a Pt wire counter-electrode and a Pt microdisc working electrode; Ag/AgNO<sub>3</sub> couple as the pseudo-reference electrode. See ESI, Fig. S1 for the voltammograms. <sup>f</sup> Excited-state reduction potential:  $E_{\text{red}}^* = E_{\text{red}} + \Delta E_{\text{T}}$ . <sup>g</sup> Phosphorescence lifetimes observed at  $\lambda_{\text{em}} = 518 \text{ nm}$  (Irdfppy), 481 nm (IrdCF3), 545 nm (Irfppy), 525 nm (Irpbt), 582 nm (Irppy), 600 nm (Irbtp) and 659 nm (IrOMe). <sup>h</sup> Photoluminescence quantum yields. <sup>i</sup> Radiative rate constant:  $k_{\text{r}} = \text{PLQY}/\tau$ . <sup>j</sup> Nonradiative rate constant:  $k_{\text{nr}} = (1 - \text{PLQY})/\tau$ .

and 2, respectively. The compounds were prepared according to the synthetic protocols which we reported previously.<sup>33,54</sup> ADTE was newly added to our DTE series, and fully characterized by standard spectroscopic identification techniques (see ESI†). The closed form of DTE compounds featured distinct visible absorption bands at 591 nm (PDTEc,  $\epsilon = 9940 \text{ M}^{-1} \text{ cm}^{-1}$ ), 586 nm (PhDTEc,  $\epsilon = 12\,500 \text{ M}^{-1} \text{ cm}^{-1}$ ), 593 nm (MDTEc,  $\epsilon = 20\,100 \text{ M}^{-1} \text{ cm}^{-1}$ ), 599 nm (CDTEc,  $\epsilon = 21\,400 \text{ M}^{-1} \text{ cm}^{-1}$ ) and

634 nm (ADTEc,  $\epsilon = 16\,700 \text{ M}^{-1} \text{ cm}^{-1}$ ). The DTEc compounds underwent photochromic cycloreversion upon photoirradiation at  $\lambda > 500 \text{ nm}$  (300 W), with  $\text{PCQY}_{\text{C} \rightarrow \text{O}}$  values ranging from 0.013 to 0.016 (Table 2). These values were one order of magnitude smaller than  $\text{PCQY}_{\text{O} \rightarrow \text{C}}$  (0.16–0.46; Table 2), demonstrating the low efficiencies for the photochromic cycloreversion.

Photoelectrocatalytic cycloreversion was performed for Ar-saturated  $\text{CH}_3\text{CN}$  solutions containing 1.0 mM Ir(III) complex

Table 2 Photophysical and electrochemical data for the DTE compounds<sup>a</sup>


	$\lambda_{\text{abs}}^b/\text{nm}$ ( $\epsilon/10^3 \text{ M}^{-1} \text{ cm}^{-1}$ )		$E_{\text{ox}}^c$ (vs. SCE)/V		Conversion yields <sup>d</sup> (%)		PCQY <sup>e</sup> (%)	
	DTEo	DTEc	DTEo	DTEc	Closing	Opening	Closing	Opening
PDTE	302 (27.6)	591 (9.94), 379 (6.43), 272 (18.9)	2.70 <sup>f</sup>	1.00	89	Quant <sup>g</sup>	39	1.6
PhDTE	286 (29.4)	586 (12.5), 381 (8.21), 309 (21.5)	1.54	0.90	87	Quant <sup>g</sup>	46	1.5
MDTE	297 (43.5)	593 (20.1), 346 (27.8), 265 (12.9)	1.24	0.72	94	Quant <sup>g</sup>	37	1.5
CDTE	308 (37.2)	599 (21.4), 379 (24.9), 319 (16.9)	1.15	0.69	91	Quant <sup>g</sup>	36	1.4
ADTE	332 (33.6)	634 (16.7), 414 (14.5), 323 (13.8)	0.63 <sup>h</sup>	0.27 <sup>h</sup>	61	83	16	1.3

<sup>a</sup> Some data were taken from ref. 33. <sup>b</sup> 10  $\mu\text{M}$  DTE in acetonitrile, 298 K. <sup>c</sup> Oxidation potential determined by cyclic voltammetry. *Conditions:* scan rate = 100  $\text{mV s}^{-1}$ ; 1.0 mM in an Ar-saturated acetonitrile containing 0.10 M  $\text{Bu}_4\text{NPF}_6$  supporting electrolyte; Pt wire counter and Pt microdisc working electrodes; Ag/AgNO<sub>3</sub> couple for the pseudo-reference electrode. <sup>d</sup> Determined by <sup>1</sup>H NMR spectroscopy (2.0 mM in CD<sub>3</sub>CN); closing condition, 3 h photoirradiation under  $\lambda = 254 \text{ nm}$  (4 W); opening condition, 1 h photoirradiation at  $\lambda > 500 \text{ nm}$  (300 W). <sup>e</sup> Photochromic quantum yields determined by employing PhDTE as a standard. <sup>f</sup> Calculated by  $E_{\text{ox}} = E_{\text{red}} + \Delta E_{00}$ , where  $E_{\text{red}}$  and  $\Delta E_{00}$  are the peak reduction potential and the optical bandgap energy, respectively. <sup>g</sup> Quantitative. <sup>h</sup> Confirmed by differential pulse voltammetry (ESI, Fig. S2).

and 1.0 mM DTEc at 298 K (beam-pass length = 1 mm). As shown in Fig. 1a, 420 nm photoirradiation of an acetonitrile solution of IrOMe and PhDTEc led to bleaching at the 586 nm absorption, indicating cycloreversion of PhDTEc. The reaction proceeded to completion without any byproduct formation, as proved by  $^1\text{H}$  NMR. To confirm that the cycloreversion was due to photoexcitation of IrOMe, the  $\text{PeCQY}_{\text{C}\rightarrow\text{O}}/\text{PCQY}_{\text{C}\rightarrow\text{O}}$  (*i.e.*,  $\text{QY}_{\text{C}\rightarrow\text{O}}(\text{with catalyst})/\text{QY}_{\text{C}\rightarrow\text{O}}(\text{without catalyst})$ ) ratios were recorded with varying the photoirradiation wavelength over the range of 380–450 nm. As shown in Fig. 2, the  $\text{PeCQY}_{\text{C}\rightarrow\text{O}}/\text{PCQY}_{\text{C}\rightarrow\text{O}}$  ratio exhibited the peak value around 420 nm, where the singlet metal-to-ligand charge-transfer ( $^1\text{MLCT}$ ) transition band of IrOMe was observed.<sup>54</sup> Quantum chemical calculations by the time-dependent density functional theory (uB3LYP/LANL2DZ: 6-31+G(d,p)) predicted 30% of the MLCT character of IrOMe. It was noted that the  $^1\text{MLCT}$  absorption bands of all Ir(III) complexes exhibited negligible overlap with the absorption spectra of DTEc and DTEo (ESI, Fig. S3 and S4<sup>†</sup>). Thus, any crosstalk between the photoelectrocatalytic cycloreversion ( $\lambda \sim 420$  nm) and the photochromic cyclization ( $\lambda = 254$  nm) can be ignored. As expected, the cycloreversion proceeded in a catalytic manner because full conversion of PhDTEc by 0.10 equiv. IrOMe was achieved ( $^1\text{H}$  NMR spectroscopy; 400 MHz,  $\text{CD}_3\text{CN}$  containing 0.20 mM IrOMe and 2.0 mM PhDTEc; see ESI, Fig. S5<sup>†</sup>), and the  $\text{PeCQY}_{\text{C}\rightarrow\text{O}}$  value increased sharply in proportion with the IrOMe concentration (ESI, Fig. S6<sup>†</sup>).

Having demonstrated the photoelectrocatalytic cycloreversion, we determined  $\text{PeCQY}_{\text{C}\rightarrow\text{O}}$  values for 35 combinations of five DTEc compounds and seven Ir(III) complexes (1.0 mM DTEc and 0.20 mM Ir(III) complex in Ar-saturated  $\text{CH}_3\text{CN}$ ) by using standard ferrioxalate actinometry (6.0 mM  $\text{K}_3[\text{Fe}(\text{C}_2\text{O}_4)_3]$ ).<sup>55</sup> Photoirradiation wavelengths were selected at

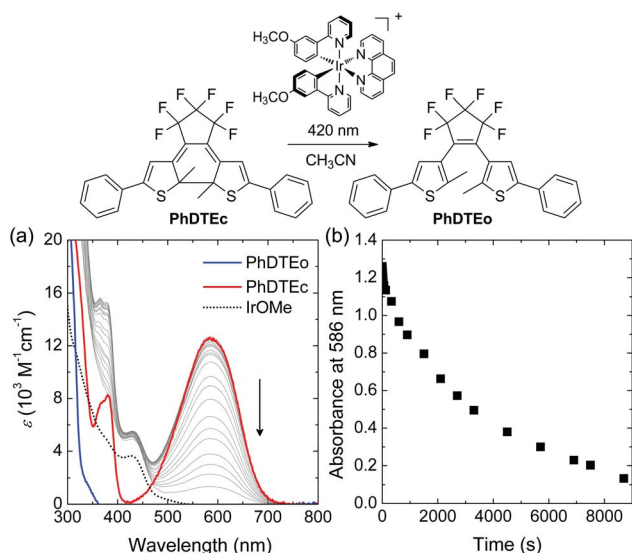


Fig. 1 Photoelectrocatalytic cycloreversion of 1.0 mM PhDTEc by photoirradiation of 1.0 mM IrOMe (Ar-saturated  $\text{CH}_3\text{CN}$ ;  $\lambda = 420$  nm ( $6.7 \times 10^{-10}$  Einstein  $\text{s}^{-1}$ )). (a) UV-vis absorption spectra: red line, PhDTEc; grey lines, PhDTEc + IrOMe during the photoirradiation; blue line, PhDTEo; dotted black line, IrOMe. (b) Decrease in the absorbance at 586 nm during the course of photoelectrocatalytic cycloreversion.

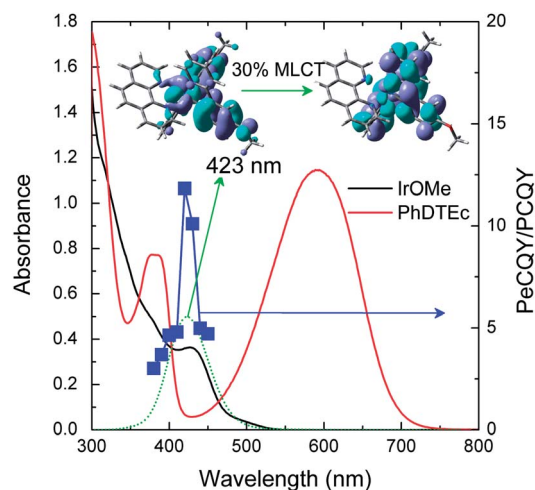


Fig. 2 Plots of  $\text{PeCQY}_{\text{C}\rightarrow\text{O}}/\text{PCQY}_{\text{C}\rightarrow\text{O}}$  ratios for cycloreversion of PhDTEc as a function of the photoirradiation wavelength (380–450 nm; blue squares): red line, UV-vis absorption spectrum of 1.0 mM PhDTEc; black line, UV-vis absorption spectrum of 1.0 mM IrOMe; dotted green line, simulated absorption spectrum of IrOMe (TD-DFT; uB3LYP/LANL2DZ:6-31+G(d,p)). Inset figures are molecular orbital isosurfaces that contribute to the  $^1\text{MLCT}$  transition (423 nm, percent MLCT character = 30%).

the  $^1\text{MLCT}$  transition bands of the Ir(III) complexes: Irdfppy, 410 nm ( $8.3 \times 10^{-10}$  Einstein  $\text{s}^{-1}$ ); IrDCF3, 410 nm ( $8.3 \times 10^{-10}$  Einstein  $\text{s}^{-1}$ ); Irffpy, 410 nm ( $8.3 \times 10^{-10}$  Einstein  $\text{s}^{-1}$ ); Irpbt, 420 nm ( $6.7 \times 10^{-10}$  Einstein  $\text{s}^{-1}$ ); Irppy, 410 nm ( $8.3 \times 10^{-10}$  Einstein  $\text{s}^{-1}$ ); Irbtp, 420 nm ( $6.7 \times 10^{-10}$  Einstein  $\text{s}^{-1}$ ); IrOMe, 420 nm ( $6.7 \times 10^{-10}$  Einstein  $\text{s}^{-1}$ ). The  $\text{PeCQY}_{\text{C}\rightarrow\text{O}}$  values are summarized in Table 3, which shows one order of magnitude enhancement in the quantum yields over normal photochromism (*i.e.*, with no catalyst).

Two trends are observed in Table 3;  $\text{PeCQY}_{\text{C}\rightarrow\text{O}}$  increased as the ground-state reduction potential of the Ir(III) complexes decreased (rows in Table 3) and the oxidation potentials of DTEc compounds increased (columns in Table 3). These observations suggested that back electron transfer as well as forward electron transfer between DTEc and the Ir(III) complex was critically involved in the photoelectrocatalytic cycloreversion. On the contrary, the phosphorescence lifetimes of the Ir(III) complexes had a weak correlation with the  $\text{PeCQY}_{\text{C}\rightarrow\text{O}}$  values (ESI, Fig. S7<sup>†</sup>), which refuted the common prediction that a long-lifetime photoredox catalyst would be more efficient.<sup>56–58</sup> These findings obviously present the need to clarify molecular factors affecting the photoelectrocatalytic processes. Scheme 2 summarizes the proposed mechanism for photoelectrocatalytic cycloreversion which comprises three key steps of (1) generation of the radical cation of DTEc ( $\text{DTEc}^{\bullet+}$ ), (2) cycloreversion of  $\text{DTEc}^{\bullet+}$  to the radical cation of DTEo ( $\text{DTEo}^{\bullet+}$ ), and (3) reductive termination to DTEo with the generation of the ground state or the excited state of the catalyst.

### Generation of the radical intermediate

Photon absorption by the  $^1\text{MLCT}$  transition of the Ir(III) complex,  $[\text{Ir}^{\text{III}}(\text{CAN})_2\text{phen}]^+$ , promotes the electronic

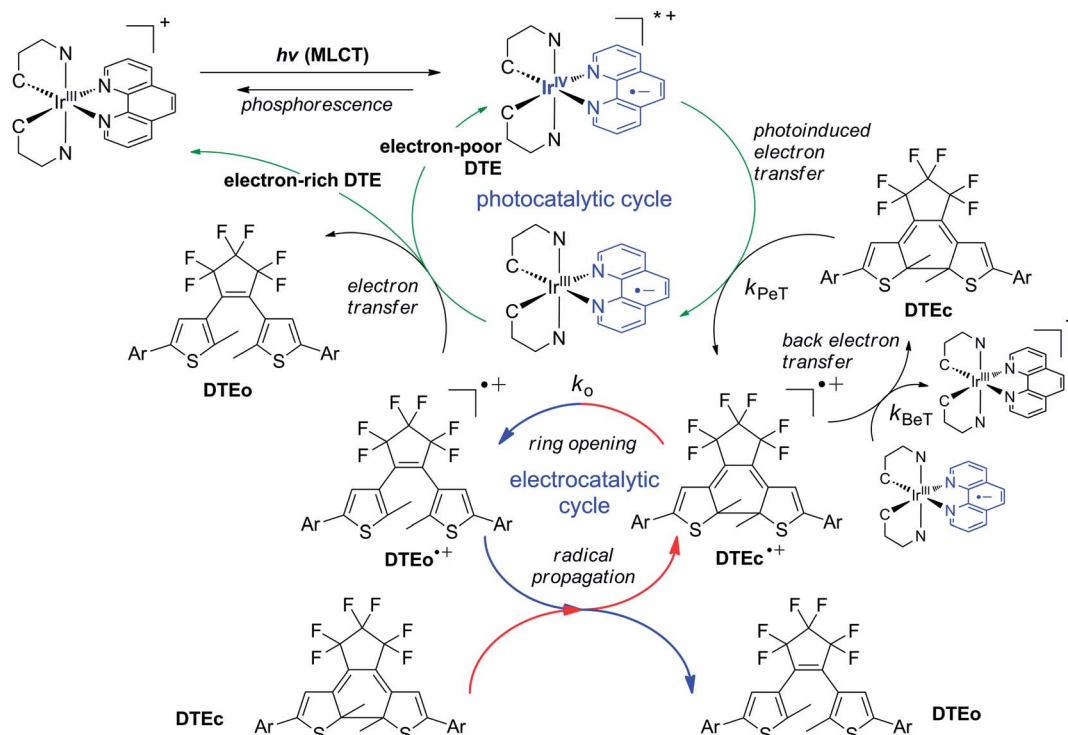
Table 3 Quantum yields for the photoelectrocatalytic cycloversion (PeCQY<sub>C→O</sub>) of DTEc compounds (%)<sup>a</sup>

	IrdCF3 (−1.27 V <sup>b</sup> )	Irbtp (−1.28 V <sup>b</sup> )	Irdfppy (−1.30 V <sup>b</sup> )	Irpbt (−1.31 V <sup>b</sup> )	Irfppy (−1.34 V <sup>b</sup> )	Irppy (−1.37 V <sup>b</sup> )	IrOMe (−1.38 V <sup>b</sup> )	No catalyst
PDTEc (1.00 V <sup>c</sup> )	26	28	34	36	35	37	38	1.6
PhDTEc (0.90 V <sup>c</sup> )	10	15	18	18	18	20	21	1.5
MDTEc (0.72 V <sup>c</sup> )	6.0	8.0	11	11	14	16	17	1.4
CDTEc (0.69 V <sup>c</sup> )	13	16	17	17	19	23	22	1.4
ADTEc (0.27 V <sup>c</sup> )	4.0	9.0	10	10	12	12	19	1.2

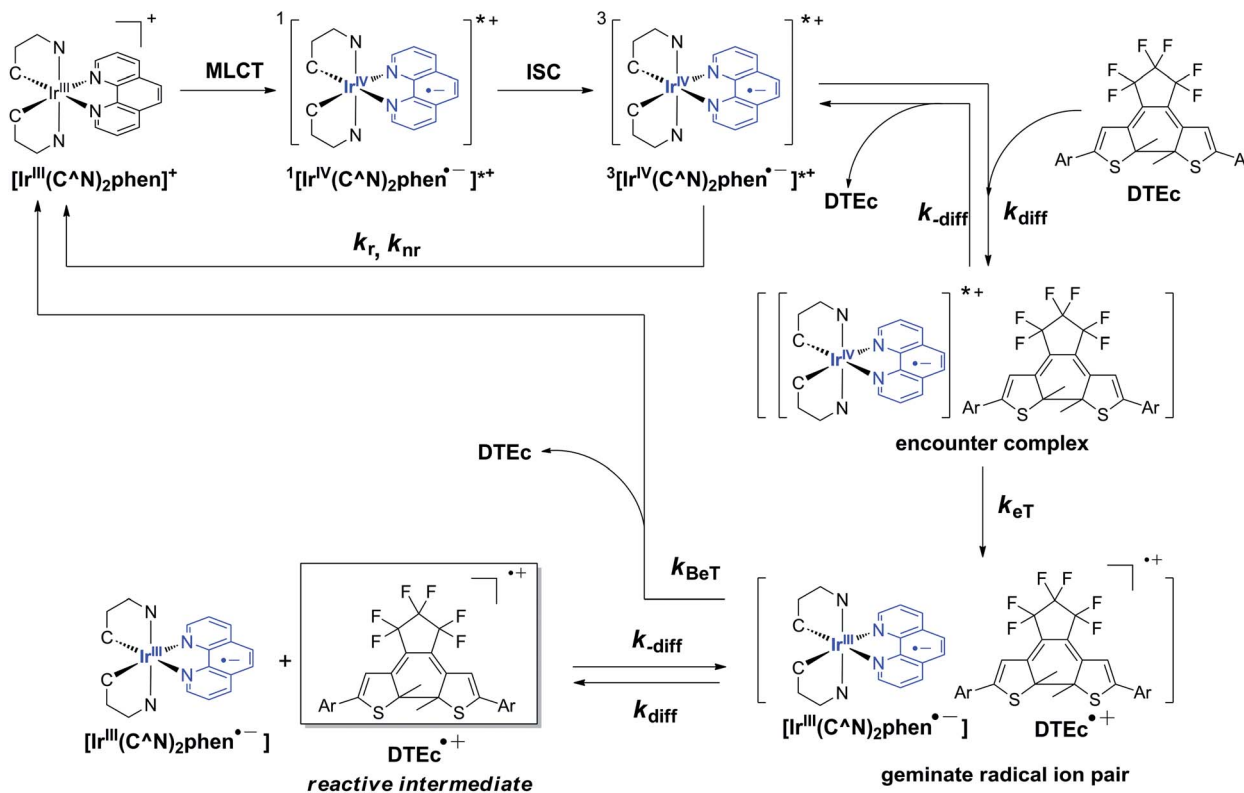
<sup>a</sup> Determined by standard ferrioxalate actinometry (6.0 mM K<sub>3</sub>[Fe(C<sub>2</sub>O<sub>4</sub>)<sub>3</sub>], QY = 1.1 at 410 and 420 nm). *Conditions:* 0.20 mM photoredox catalyst and 1.0 mM DTEc in deaerated CH<sub>3</sub>CN. Photoirradiation wavelength: IrdCF3, 410 nm (8.3 × 10<sup>−10</sup> Einstein s<sup>−1</sup>); Irbtp, 420 nm (6.7 × 10<sup>−10</sup> Einstein s<sup>−1</sup>); Irdfppy, 410 nm (8.3 × 10<sup>−10</sup> Einstein s<sup>−1</sup>); Irpbt, 420 nm (6.7 × 10<sup>−10</sup> Einstein s<sup>−1</sup>); Irfppy, 410 nm (8.3 × 10<sup>−10</sup> Einstein s<sup>−1</sup>); Irppy, 410 nm (8.3 × 10<sup>−10</sup> Einstein s<sup>−1</sup>); IrOMe, 420 nm (6.7 × 10<sup>−10</sup> Einstein s<sup>−1</sup>); no catalyst, 410 nm (8.3 × 10<sup>−10</sup> Einstein s<sup>−1</sup>). <sup>b</sup> E<sub>red</sub> of the Ir(III) complex (vs. SCE, V). <sup>c</sup> One-electron oxidation potential of DTEc (vs. SCE, V).

transition from the d-orbital of the Ir(III) core to the π\*-orbital of the ligand (i.e., <sup>1</sup>[Ir<sup>IV</sup>(CAN)(CAN)-phen]<sup>++</sup> or <sup>1</sup>[Ir<sup>IV</sup>(CAN)<sub>2</sub>phen]<sup>++</sup>). Subsequent intersystem crossing affords the triplet MLCT (<sup>3</sup>MLCT) transition state (i.e., <sup>3</sup>[Ir<sup>IV</sup>(CAN)(CAN)-phen]<sup>++</sup> or <sup>3</sup>[Ir<sup>IV</sup>(CAN)<sub>2</sub>phen]<sup>++</sup>) at rates faster than 100 fs,<sup>59,60</sup> which is responsible for the oxidation of DTEc. The one-electron reduction potentials (E<sub>red</sub><sup>\*</sup>) of the triplet species of the Ir complexes are 1.01–1.52 V (vs. SCE, Table 1), being more positive than the E<sub>ox</sub> values of the DTEc compounds (0.27–1.00 V vs. SCE, Table 2). Thus exergonic photoinduced electron transfer (PeT) from DTEc to the photoredox catalyst with positive driving force (−ΔG<sub>PeT</sub> = e[E<sub>ox</sub>(DTEc) − E<sub>red</sub><sup>\*</sup>(Ir)] = 0.01–1.25 eV) is anticipated within an encounter complex (Scheme 3).<sup>61–63</sup>

Strong phosphorescence emission (PLQY = 1–21%) of the Ir(III) complexes allowed the determination of the rate constants for PeT (k<sub>PeT</sub>) by measuring the decrease in the phosphorescence lifetimes (τ, λ<sub>ex</sub> = 377 nm). Fig. 3a displays the phosphorescence decay profiles (λ<sub>em</sub> = 525 nm) of 100 μM Irpbt in Ar-saturated CH<sub>3</sub>CN solutions containing various concentrations (0–40 μM) of PhDTEc. The τ value was as long as 4.07 μs in the absence of PhDTEc, decreasing in proportion with the PhDTEc concentration. The decrease in τ was attributed to occurrence of PeT that competed with the radiative decay. A linear fit for the electron transfer rate, 1/τ − 1/τ<sub>0</sub> (τ and τ<sub>0</sub> are phosphorescence lifetimes in the presence and the absence of PhDTEc), vs. the PhDTEc concentration afforded the bimolecular electron transfer rate constant to be 4.58 × 10<sup>9</sup> M<sup>−1</sup> s<sup>−1</sup>



Scheme 2 Proposed mechanism for the photoelectrocatalytic cycloversion of DTEc compounds by Ir(III) complexes as the photoredox catalysts.



Scheme 3 Generation of the radical intermediate by photoredox catalysis.

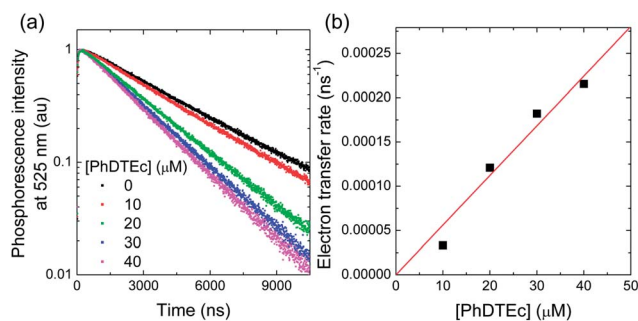


Fig. 3 Determination of the rate constant for photoinduced electron transfer ( $k_{\text{PeT}}$ ) from PhDTEc to Irpbt. (a) Phosphorescence decay traces of 100  $\mu\text{M}$  Irpbt in Ar-saturated  $\text{CH}_3\text{CN}$  solutions containing 0–40  $\mu\text{M}$  PhDTEc after 377 nm nanosecond pulsed photoexcitation ( $\lambda_{\text{obs}} = 525$  nm). (b) Plot of the electron transfer rate as a function of the PhDTEc concentration. The electron transfer rate was calculated by the relationship, electron transfer rate =  $1/\tau - 1/\tau_0$ , where  $\tau$  and  $\tau_0$  are the phosphorescence lifetimes of Irpbt in the presence and the absence of PhDTEc, respectively. The slope corresponds to  $k_{\text{PeT}}$ . See ESI, Fig. S8 and S9† for plots of other combinations of the DTEc compounds and Ir complexes.

(Fig. 3b). The  $k_{\text{PeT}}$  values for other combinations of Ir(III) complexes and DTEc compounds were also determined, and fell within the range of  $10^9$  to  $10^{10} \text{ M}^{-1} \text{ s}^{-1}$  (ESI, Table S1†). The  $k_{\text{PeT}}$  values approached to the diffusion rate constant ( $k_{\text{diff}}$ ) in  $\text{CH}_3\text{CN}$  at 298 K,  $1.93 \times 10^{10} \text{ M}^{-1} \text{ s}^{-1}$ , which was calculated by the Stokes–Einstein–Smoluchowski equation,  $k_{\text{diff}} = (8k_{\text{B}}N_{\text{A}}T)/(3\eta)$ , where  $k_{\text{B}}$ ,  $N_{\text{A}}$ ,  $T$  and  $\eta$  are the Boltzmann constant, the

Avogadro's number, the absolute temperature and viscosity of the solvent, respectively. As shown in Fig. 4, plots of  $k_{\text{PeT}}$  vs.  $-\Delta G_{\text{PeT}}$  for PDTEc features a typical Rehm–Weller behavior,<sup>63</sup> being consistent with our previous observation of PeT in a series of phosphorescent zinc sensors, where the di(2-picoly)l amino group served as a one-electron donor.<sup>54,64</sup> The  $k_{\text{PeT}}$  values adhered well to the theoretical curve obtained from the classical Marcus theory for adiabatic outer-sphere electron transfer, after taking the diffusion process into account (eqn (1); also see Scheme 3).<sup>62,65</sup>

$$k_{\text{PeT}} = \frac{k_{\text{diff}}k_{\text{eT}}}{k_{\text{-diff}} + k_{\text{eT}}} = \frac{k_{\text{diff}}Z \exp\left[-(\Delta G_{\text{PeT}} + \lambda)^2/(4\lambda k_{\text{B}}T)\right]}{k_{\text{-diff}} + Z \exp\left[-(\Delta G_{\text{PeT}} + \lambda)^2/(4\lambda k_{\text{B}}T)\right]} \quad (1)$$

In eqn (1),  $Z$  and  $\lambda$  are the collisional frequency taken as  $1.0 \times 10^{11} \text{ M}^{-1} \text{ s}^{-1}$  and the reorganization energy for the one-electron oxidation of DTEc, respectively.<sup>66</sup> The  $k_{\text{PeT}}$  values of PDTEc overlap with the kinks of the theoretical curves of eqn (1) having  $\lambda$  values between 0.60 and 0.90 eV, because the  $\lambda$  value increases with increasing  $-\Delta G_{\text{PeT}}$  accompanied by an increase in the distance between electron donor and acceptor molecules, where the electron transfer occurs, according to eqn (2).

$$\lambda_{\text{s}} = \frac{(\Delta e)^2}{4\pi\epsilon_0} \left( \frac{1}{2r_{\text{D}}} + \frac{1}{2r_{\text{A}}} - \frac{1}{d} \right) \left( \frac{1}{\epsilon_{\text{op}}} - \frac{1}{\epsilon_{\text{s}}} \right) \quad (2)$$

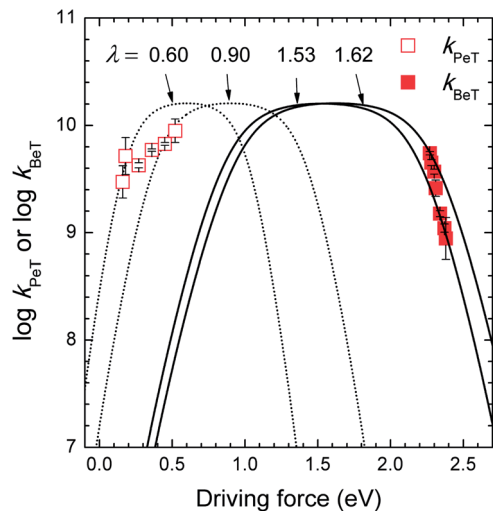


Fig. 4 Plots of  $\log k_{\text{PeT}}$  vs.  $-\Delta G_{\text{PeT}}$  (empty symbols) and  $\log k_{\text{BeT}}$  vs.  $-\Delta G_{\text{BeT}}$  (filled symbols) for photoelectrocatalytic cycloreversion of PDTEc by the Ir complexes at 298 K. Dotted and solid curves are the theoretical plots of eqn (1) at  $k_{\text{diff}} = 1.93 \times 10^{10} \text{ M}^{-1} \text{ s}^{-1}$ .

In eqn (2),  $\lambda_s$  is the solvent reorganization energy,  $\Delta e$  is the amount of transferred charge ( $\Delta e = e$ ),  $\epsilon_0$  is the dielectric constant in a vacuum,  $r_A$  and  $r_D$  are the van der Waals radii of electron donor and acceptor molecules,  $d$  is the contact distance,  $\epsilon_{\text{op}}$  is the optical dielectric constant, and  $\epsilon_s$  is the dielectric constant of the solvent, respectively. Such an increase in the  $\lambda$  values with increasing  $-\Delta G_{\text{PeT}}$  has previously been reported for PeT from the triplet excited state of cofacial porphyrin dimers to a series of electron acceptors.<sup>67</sup>

The Marcus-normal behavior (*i.e.*,  $-\Delta G_{\text{PeT}} < \lambda$ ) suggests one viable strategy to improving PeT efficiencies although the effect may be marginal; faster PeT could be obtainable by increasing  $E_{\text{red}}^*$  of the Ir(III) complex. This strategy requires synthetic modifications to increasing  $\Delta E_{\text{T}}$  and  $E_{\text{red}}$ , which can be accomplished by using high-field ligands, such as N-heterocyclic carbene ligands, having electron-withdrawing substituents.

The one-electron reduced species of the Ir(III) complex (*i.e.*,  $[\text{Ir}^{\text{III}}(\text{CAN})_2\text{phen}^{\cdot-}]$  in Scheme 3) can promptly return its extra electron to vicinal DTEc<sup>•+</sup> in the geminate radical ion pair due to the strong reduction power of  $E_{\text{red}} < -1.27 \text{ V}$  (*vs.* SCE). Indeed, the driving force for this back electron transfer ( $-\Delta G_{\text{BeT}} = e[E_{\text{red}}(\text{Ir}) - E_{\text{ox}}(\text{DTEc})]$ ) was as large as 1.54–2.38 eV. Since this back electron transfer (BeT) served as an energy-wasting path, investigations into the effects of BeT would be very important. We thus determined the rate constant for back electron transfer ( $k_{\text{BeT}}$ ) by laser flash photolysis. Fig. 5a displays the transient absorption spectra of 500  $\mu\text{M}$  PDTEc in an Ar-saturated  $\text{CH}_3\text{CN}$  solution containing 100  $\mu\text{M}$  Irpbt recorded at various delay times after nanosecond pulsed photoexcitation ( $\lambda_{\text{ex}} = 426 \text{ nm}$ ). The absorption spectra exhibited a NIR absorption band at 810 nm. The 810 nm band was assigned due to PDTEc<sup>•+</sup> because the spectral signature coincided with the absorption spectrum for PDTEc<sup>•+</sup> (electrochemically generated at 10 °C using  $\text{Cu}(\text{ClO}_4)_2$  as an one-electron oxidant) obtained by stopped-flow UV-vis-NIR measurements and the simulated electronic absorption

spectrum for PDTEc<sup>•+</sup> (uB3LYP/6-311+G(d,p):C-PCM solvation model parameterized for acetonitrile) (Fig. 5c). The weak transient absorption precluded further spectral resolution, but all the DTEc compounds exhibited the characteristic NIR absorption behaviors. NIR absorption bands corresponding to DTEc<sup>•+</sup> have also been observed by us<sup>33</sup> and the Kawai group.<sup>44</sup> Transient absorption due to the radical anion of phen ligand ( $\text{phen}^{\cdot-}$ ) at 350 and 550 nm that have been identified for Cu(I) complexes of phen was not detected,<sup>58,68</sup> presumably due to the strong electronic coupling with the Ir core. The decay of the absorption band at 810 nm can be ascribed to BeT from the one-electron reduced species of the Ir(III) complex to PDTEc<sup>•+</sup> because the subsequent cycloreversion of PDTEc<sup>•+</sup> to PDTEo<sup>•+</sup> is much slower than BeT (*vide infra*). The  $k_{\text{BeT}}$  value for the PDTEc<sup>•+</sup>/Irpbt pair was thus obtained from the second-order linear fit of the temporal changes of  $\epsilon$ /absorbance values at 810 nm to be  $2.6 \pm 0.5 \times 10^9 \text{ M}^{-1} \text{ s}^{-1}$ , where  $\epsilon$  for PDTEc<sup>•+</sup> was calculated from the stopped-flow UV-vis-NIR spectrum (Fig. 5c). Similarly, the  $k_{\text{BeT}}$  value of  $7.3 \pm 0.2 \times 10^9 \text{ M}^{-1} \text{ s}^{-1}$  for the ADTEc<sup>•+</sup>/Irpbt pair was determined by measuring the NIR transient absorption band of ADTEc<sup>•+</sup> at 1000 nm (Fig. 5d–f). Table 4 lists the  $k_{\text{BeT}}$  values for 35 combinations of the Ir(III) complexes and DTEc compounds. Inspection of Tables 3 and 4 reveals that  $\text{PeCQY}_{\text{C} \rightarrow \text{O}}$  increases when  $k_{\text{BeT}}$  decreases, which suggests the critical role of BeT.

As shown in Fig. 4, a strong negative dependence between  $k_{\text{BeT}}$  and  $-\Delta G_{\text{BeT}}$  was observed. Our system presents a rare example featuring the Marcus-normal PeT and the Marcus-inverted BeT.<sup>65,69–71</sup> The occurrence of BeT in the Marcus-inverted region may explain the larger  $\text{PeCQY}_{\text{C} \rightarrow \text{O}}$  values for higher exothermicities of BeT (ESI, Fig. S15<sup>†</sup>),<sup>69,72–93</sup> because the lifetime of DTEc<sup>•+</sup> becomes longer for cycloreversion. The Marcus-inverted BeT provides an important design criterion that  $E_{\text{red}}$  of the photoredox catalyst should be as negative as possible. In addition, the stronger dependence of  $k_{\text{BeT}}$  to the driving force compared to the case of  $k_{\text{PeT}}$  suggests that control of  $E_{\text{red}}$  rather than  $E_{\text{red}}^*$  would be crucial to achieving high quantum yields. The plots of  $\log k_{\text{BeT}}$  vs.  $-\Delta G_{\text{BeT}}$  were well-fitted to the Marcus theory of adiabatic outer-sphere electron transfer (eqn (1)). The best fits were obtained at  $\lambda$  values of 1.59 eV (PDTEc), 1.57 eV (PhDTEc), 1.43 eV (MDTEc), 1.39 eV (CDTEc) and 1.07 eV (ADTEc) (Fig. 4 and ESI, S16<sup>†</sup>). Apparently, DTEc having the electron-withdrawing moieties are found to have larger  $\lambda$ , which may result from the larger structural change associated with the electron transfer, leading to greater propensity for cycloreversion of DTEc<sup>•+</sup> to DTEo<sup>•+</sup>. However, such a change in the  $\lambda$  value for the forward electron transfer is masked by the diffusion-limited rate (Fig. 4).

### Ring-opening reaction of the radical intermediate

To decouple the ring-opening process with PeT and BeT, DTEc<sup>•+</sup> was generated by the electron transfer oxidation of DTEc with  $\text{Cu}(\text{ClO}_4)_2$  used as an one-electron oxidant,<sup>33</sup> and the ring-opening process was monitored by single-mixing stopped-flow UV-vis absorption changes of DTEc<sup>•+</sup> recorded at 100 ms intervals ( $\text{CH}_3\text{CN}$ , 10 °C). The NIR absorption at  $\lambda > 700 \text{ nm}$  for

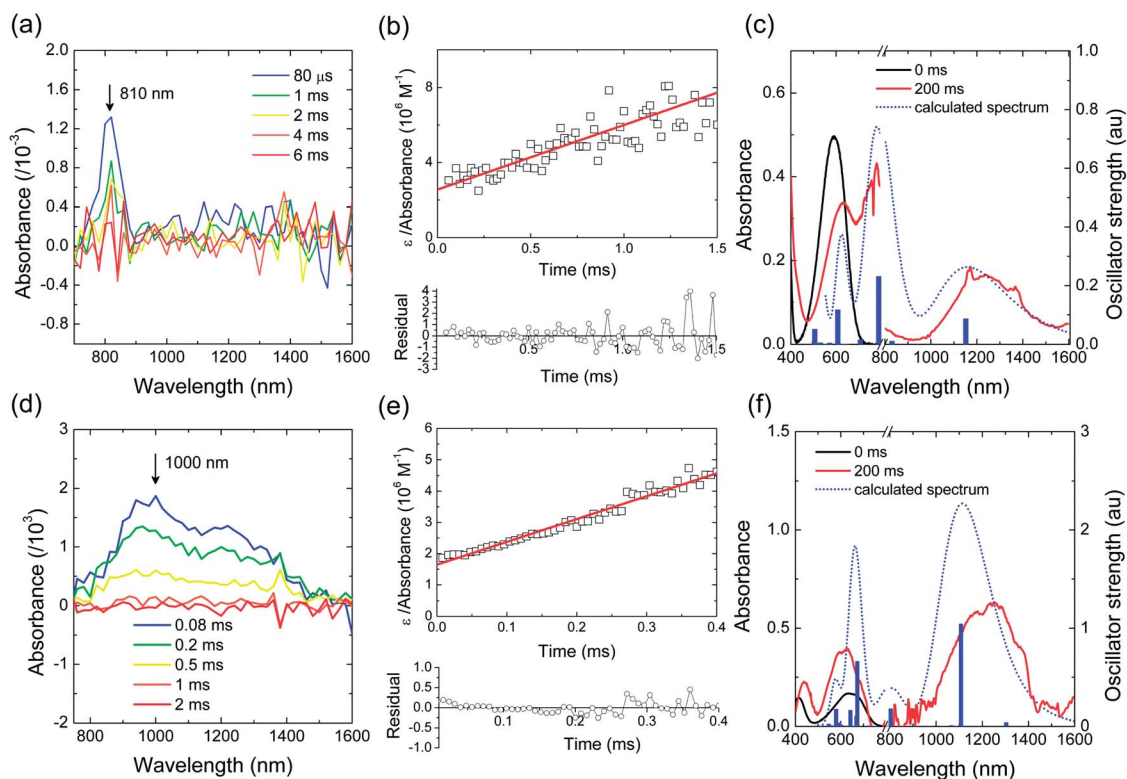


Fig. 5 Laser flash photolysis to determine the rate constants for back electron transfer (Ar-saturated  $\text{CH}_3\text{CN}$ , 426 nm nanosecond photoexcitation). Top panels, 500  $\mu\text{M}$  PDTEc and 100  $\mu\text{M}$  Irpbt: (a) transient absorption spectra, (b) plot of  $\epsilon/\text{absorbance}$  at the 810 nm band vs. time, and (c) stopped-flow UV-vis-NIR absorption spectra (10  $^\circ\text{C}$ ) of 50  $\mu\text{M}$  PDTEc (black) and electrochemically generated PDTEc $^{+\cdot}$  (red; 50  $\mu\text{M}$  PDTEc + 4 equiv. of  $\text{Cu}(\text{ClO}_4)_2$ ) and TD-DFT-calculated UV-vis-NIR electronic absorption spectra for PDTEc $^{+\cdot}$  (blue). Lower panels, 500  $\mu\text{M}$  ADTEc and 100  $\mu\text{M}$  Irpbt: (d) transient absorption spectra, (e) plot of  $\epsilon/\text{absorbance}$  at the 1000 nm band vs. time, and (f) stopped-flow UV-vis-NIR absorption spectra (10  $^\circ\text{C}$ ) of 10  $\mu\text{M}$  ADTEc (black) and electrochemically generated ADTEc $^{+\cdot}$  (red; 10  $\mu\text{M}$  ADTEc + 4 equiv. of  $\text{Cu}(\text{ClO}_4)_2$ ) and TD-DFT-calculated UV-vis-NIR electronic absorption spectra for ADTEc $^{+\cdot}$  (blue). For other combinations of DTEc compounds and Ir(III) complexes, see ESI, Fig. S10–S14.†

PhDTEc $^{+\cdot}$  appeared promptly after the addition of 4 equiv.  $\text{Cu}(\text{ClO}_4)_2$  to 50  $\mu\text{M}$  PhDTEc, which accompanied the disappearance of the PhDTEc absorption band at 586 nm (Fig. 6). The NIR absorption band of PhDTEc $^{+\cdot}$  decayed at a rate of 0.17  $\text{s}^{-1}$ , the value being comparable to our previous results.<sup>33</sup>

Absorption around 540 nm presumably due to PhDTEo $^{+\cdot}$  was detected, but the significant overlap with the PhDTEc absorption did not permit clear resolution. Thus, the unimolecular rate constant ( $k_o$ ) for PhDTEc $^{+\cdot} \rightarrow$  PhDTEo $^{+\cdot}$  was determined from the PhDTEc $^{+\cdot}$  decay rate to be 0.17  $\text{s}^{-1}$ . This  $k_o$  value is much smaller than  $k_{\text{PeT}}$  and  $k_{\text{BeT}}$  by factors of  $10^6$  to  $10^7$  at 1.0

mM concentration of PhDTE, implying that cycloreversion of PhDTEc $^{+\cdot}$  is the rate-determining step in the overall photoelectrocatalytic cycloreversion reaction. The  $k_o$  values for other DTEc compounds were determined similarly at 10  $^\circ\text{C}$  (ESI, Fig. S17–S21†): PDTE, 0.061  $\text{s}^{-1}$ ; MDTE, 0.35  $\text{s}^{-1}$ ; CDTE, 2.2  $\text{s}^{-1}$ ; ADTE, 5.7  $\text{s}^{-1}$ . To obtain the thermodynamic information about the cycloreversion of DTEc $^{+\cdot}$ ,  $k_o$  values were also measured at  $-10$  and  $0$   $^\circ\text{C}$  (ESI, Fig. S17–S21†). Eyring plots of  $\log [(h/k_B)(k_o/T)]$  vs.  $1/T$  follow straight lines with activation enthalpy ( $\Delta H^\ddagger$ ) values of 0.74 eV (PDTEc), 0.61 eV (PhDTEc), 0.42 eV (MDTEc), 0.36 eV (CDTEc) and 0.34 eV (ADTEc) (Fig. 7). The smallest  $\Delta H^\ddagger$

Table 4 Back electron-transfer rate constants ( $k_{\text{BeT}}$ ,  $10^9 \text{ M}^{-1} \text{ s}^{-1}$ ) for the photoelectrocatalytic cycloreversion of DTEc compounds by Ir complexes<sup>a</sup>

	IrdCF3	Irbtp	Irdfppy	Irpbt	Irfppy	Irppy	IrOMe	$\lambda^b$ /eV
PDTE	$5.5 \pm 0.2$	$4.5 \pm 0.3$	$3.7 \pm 0.2$	$2.6 \pm 0.5$	$1.5 \pm 0.1$	$1.1 \pm 0.1$	$0.88 \pm 0.5$	$1.59 \pm 0.06$
PhDTE	$8.0 \pm 0.3$	$6.0 \pm 0.2$	$5.2 \pm 1.2$	$4.5 \pm 0.6$	$2.9 \pm 0.7$	$2.7 \pm 0.7$	n.d. <sup>c</sup>	$1.57 \pm 0.03$
MDTE	$12 \pm 0.2$	$5.5 \pm 0.2$	$6.2 \pm 1.0$	$4.1 \pm 0.5$	$5.9 \pm 0.6$	$2.2 \pm 0.7$	$2.17 \pm 0.2$	$1.43 \pm 0.05$
CDTE	$9.4 \pm 0.2$	$6.3 \pm 1.0$	$5.5 \pm 0.3$	$4.5 \pm 1.0$	$2.8 \pm 0.2$	$2.2 \pm 0.6$	n.d. <sup>c</sup>	$1.39 \pm 0.03$
ADTE	$9.4 \pm 0.3$	$9.1 \pm 0.2$	$8.5 \pm 0.3$	$7.3 \pm 0.2$	$4.6 \pm 0.04$	$3.6 \pm 0.06$	$3.2 \pm 0.2$	$1.07 \pm 0.01$

<sup>a</sup> Determined by nanosecond laser flash photolysis. <sup>b</sup> Reorganization energy. <sup>c</sup> Not determined.

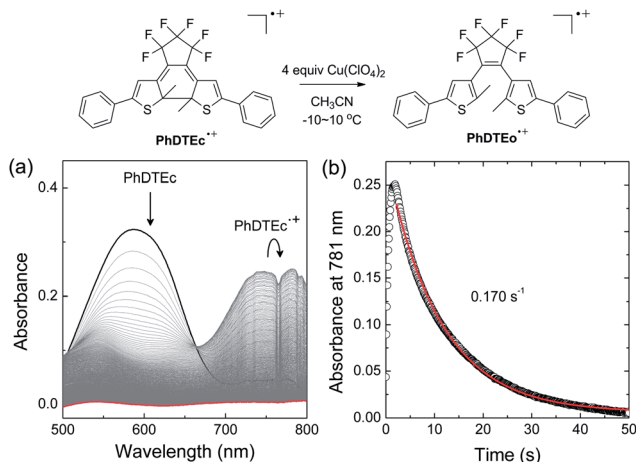


Fig. 6 Determination of the rate constant for the ring-opening reaction ( $k_o$ ) of PhDTEc $^{\bullet+}$ : (a) stopped flow UV-vis absorption spectra (single mixing) of 50  $\mu$ M PhDTEc after mixing with 4 equiv. Cu(ClO $_4$ ) $_2$  at 10  $^\circ$ C (CH $_3$ CN) and (b) decay traces of the 781 nm absorption band of PhDTEc $^{\bullet+}$ .

value was obtained for ADTEc, and the value increased in proportion with the electron deficiency. This trend is obviously opposite to the results in the PeCQY $_{C \rightarrow O}$  ordering (Table 3). This discrepancy may be explained by the mechanism concerning the termination steps (*vide infra*).

### Radical propagation and termination

Scheme 4 summarizes possible paths for the reduction of DTEo $^{\bullet+}$  to DTEo; DTEo $^{\bullet+}$  is neutralized by accepting one electron from DTEc or the one-electron reduced species of the Ir complex, [Ir $^{III}$ (C $\wedge$ N) $_2$ phen $^{\bullet-}$ ]. The former and the latter reductive electron transfer pathways correspond to radical propagation and termination steps, respectively. The propagation step by electron transfer from DTEc to DTEo $^{\bullet+}$  is moderately exergonic judging from the driving force for propagation ( $-\Delta G_p$ ,  $-\Delta G_p = e[E_{ox}(DTEc) - E_{ox}(DTEo)]$ ) of 0.34 eV (ADTE), 0.46 eV (CDTE), 0.52 eV (MDTE), 0.64 eV (PhDTE) and 1.70 eV (PDTE). In such a case, the electron transfer process for the radical

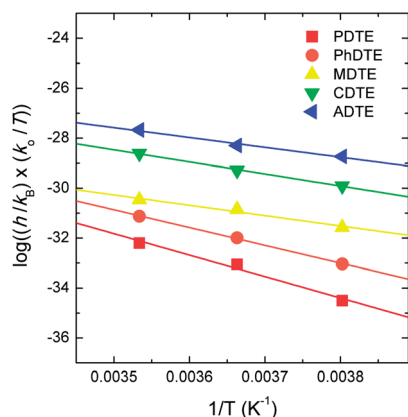
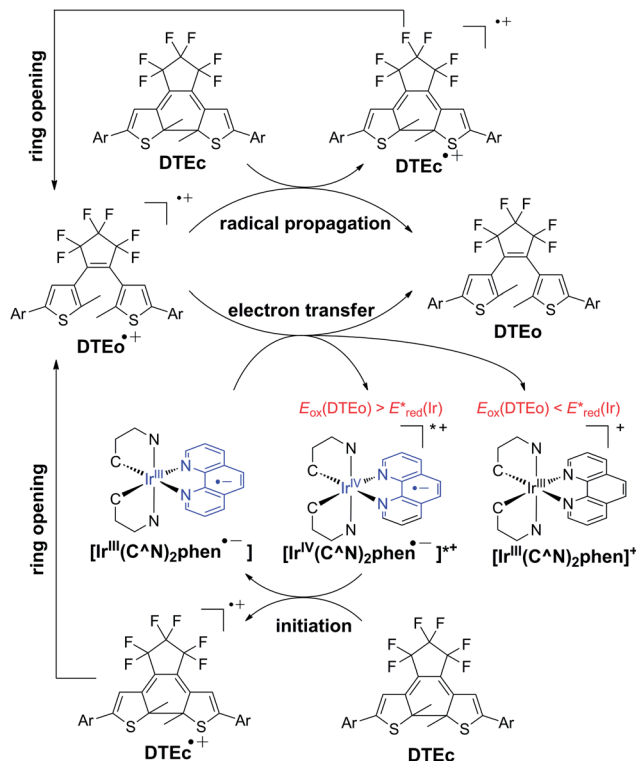


Fig. 7 Plots of  $\log[(h/k_B)(k_o/T)]$  vs.  $1/T$  for cycloreversion of DTEc $^{\bullet+}$ .



Scheme 4 Radical propagation and termination of the photoelectrocatalytic cycloreversion.

propagation may occur in the Marcus-normal region, where the propagation rate becomes faster with more electron-withdrawing substituents to reach the diffusion-limited value. The driving force for the termination step ( $-\Delta G_t$ ,  $-\Delta G_t = e[E_{red}(Ir) - E_{ox}(DTEo)]$ ) was determined to be 1.80–4.08 eV (Tables 1 and 2), being highly exergonic. The very large  $-\Delta G_t$  values suggest that termination would likely be located in the Marcus-inverted region particularly for PDTE. In the case of PDTE, BeT from the reduced Ir complex to PDTEo $^{\bullet+}$  may generate the excited state of the Ir complex rather than the ground state because  $-\Delta G_t$  (3.97–4.08 eV) is significantly larger than the triplet excited-state energies of the Ir(III) complexes ( $\Delta E_T$ , 2.39–2.82 eV). Actually, very weak delayed phosphorescence emission of Irfpfy was detected for Ar-saturated CH $_3$ CN solutions containing 100  $\mu$ M Irfpfy and 100  $\mu$ M PDTEc *ca.* 10 s after the 410 nm photo-irradiation (ESI, Fig. S22 $^\dagger$ ), supporting the hypothesis that the triplet excited state of the photoredox catalyst was regenerated. In such a case, the BeT process becomes not the termination step, as the recycled excited species of the photoredox catalyst can start the initiation step of electron transfer from PDTEc again, leading to significant elongation of the chain length. On the contrary, such a regeneration process is prohibited for ADTE (ESI, Fig. S22 $^\dagger$ ), because the  $-\Delta G_t$  values (1.90–2.01 eV) are smaller than the  $\Delta E_T$  values (2.39–2.82 eV) of the photoredox catalysts. This may be the reason why the PDTE afforded higher PeCQY $_{C \rightarrow O}$  values than ADTE despite the slower ring-opening rate ( $k_o$ ) of the radical intermediate. These considerations establish an important condition that  $-\Delta G_t$  should be larger

than the triplet state energy ( $\Delta E_T$ ) of the photoredox catalyst in order to achieve a larger  $\text{PeCQY}_{\text{C}\rightarrow\text{O}}$  value. This corresponds to a criterion,  $E_{\text{ox}}(\text{DTEo}) > E_{\text{red}}^*(\text{Ir})$  because  $E_{\text{red}} + \Delta E_T$  equals  $E_{\text{red}}^*$ . It can thus be concluded that BeT involved both in the generation of  $\text{DTEc}^{+\cdot}$  and in the termination to DTEo play critical roles in the overall performance of the photoelectrocatalytic cycloreversion. Collectively, the larger  $\text{PeCQY}_{\text{C}\rightarrow\text{O}}$  by IrOMe can be ascribed to the high  $E_{\text{red}}$  and the small  $\Delta E_T$  values, because these conditions effectively suppress BeT in the initiation step and facilitate regeneration of the excited species of IrOMe. Considering that the initiation by PeT is allowed only when  $E_{\text{red}}^*(\text{Ir}) > E_{\text{ox}}(\text{DTEc})$ , we can further conclude that the optimal condition for the photoelectrocatalytic action is  $E_{\text{ox}}(\text{DTEc}) < E_{\text{red}}^*(\text{Ir}) < E_{\text{ox}}(\text{DTEo})$ . This implies that DTE compounds featuring the largest difference in the oxidation potentials of the open form and the closed form are favorable for the photoelectrocatalytic cycloreversion. As shown in Table 2, PDTE has the greatest value of the electrochemical window of  $E_{\text{ox}}(\text{DTEo}) - E_{\text{ox}}(\text{DTEc})$ . Thus, it is anticipated that PDTE would retain the largest quantum yields at any choice of Ir(III) complexes, which is in excellent agreement with our experimental results (Table 3).

## Conclusions

We successfully demonstrated the highly efficient photoelectrocatalytic cycloreversion of photochromic DTE compounds. A series of cyclometalated Ir(III) complexes served as photoredox catalysts to trigger electrocatalytic cycloreversion of DTEc. Quantum yields for the photoelectrocatalytic cycloreversion were determined by ferrioxalate actinometry, and one order of magnitude enhancement relative to the controls (*i.e.*, without the photoredox catalyst) was achieved. We systemically analyzed the reaction steps in the photoelectrocatalytic cycloreversion, which consisted of photoinduced generation of the radical cation intermediate, cycloreversion of the intermediate by radical propagation, and reductive termination. We directly monitored photoinduced electron transfer and back electron transfer in the DTEc and Ir complex pairs by employing nanosecond transient photoluminescence and absorption spectroscopic techniques. The results established that the efficiency for the generation of the radical cation intermediate of DTEc ( $\text{DTEc}^{+\cdot}$ ) depended on the rate of back electron transfer occurring in the Marcus-inverted regime. It was also found that the overall quantum yields were governed not only by the efficiency for the generation of  $\text{DTEc}^{+\cdot}$  (initiation step) but also by the radical chain length for the conversion of  $\text{DTEc}^{+\cdot}$  to  $\text{DTEo}^{+\cdot}$  (propagation step), which increased in proportion with the electron deficiency of the DTE backbone as well as by the ability of the photoredox catalyst to restart the initiation step. Taken together, these findings provide useful guidance to further improving cycloreversion quantum yields: (1) the ground-state reduction potential of the photoredox catalyst should be as negative as possible to suppress BeT; (2) the excited-state reduction potential of the catalyst should be lower than the oxidation potential of DTEc to facilitate PeT, but the driving force for PeT has a marginal influence; (3) the oxidation potential of DTEc should be as positive as possible to suppress

BeT; (4) the excited-state reduction potential of the Ir complex should be smaller than the oxidation potential of DTEo to regenerate the excited species of the Ir catalyst. These conditions can be satisfied by the use of Ir(III) complexes having electron-rich cyclometalating ligands and high-field ancillary ligands, or by the use of positively charged DTEc, such as those containing pyridinium rings. We believe that our conclusions will provide valuable insight into the future development of high efficiency molecular photochromism.

## Acknowledgements

This work was supported by the CRI (W.N.), WCU (R31-2008-000-10010-0 to W.N.) and GRL (2010-00353 to W.N. and S.F.) programs from the NRF of Korea, and a Grant-in-Aid (no. 20108010 to S.F. and 23750014 to K.O.) from the MEXT of Japan, and grant from the Kyung Hee University in 2013 (KHU-20130385 to Y.Y.).

## Notes and references

- 1 B. L. Feringa, *Molecular Switches*, Wiley-VCH, Weinheim, 2001.
- 2 M. Irie, *Chem. Rev.*, 2000, **100**, 1685–1716.
- 3 M. Irie, T. Lifka, S. Kobatake and N. Kato, *J. Am. Chem. Soc.*, 2000, **122**, 4871–4876.
- 4 H. Tian and S. Yang, *Chem. Soc. Rev.*, 2004, **33**, 85–97.
- 5 A. Perrier, F. Maurel and D. Jacquemin, *Acc. Chem. Res.*, 2012, **45**, 1173–1182.
- 6 C. Yun, J. You, J. Kim, J. Huh and E. Kim, *J. Photochem. Photobiol., C*, 2009, **10**, 111–129.
- 7 S. Kawata and Y. Kawata, *Chem. Rev.*, 2000, **100**, 1777–1788.
- 8 K. Morimitsu, S. Kobatake, S. Nakamura and M. Irie, *Chem. Lett.*, 2003, **32**, 858–859.
- 9 C.-C. Ko, W. H. Lam and V. W.-W. Yam, *Chem. Commun.*, 2008, 5203–5205.
- 10 R. Göstl, B. Kobin, L. Grubert, M. Pätzelt and S. Hecht, *Chem.–Eur. J.*, 2012, **18**, 14282–14285.
- 11 J. Massaad, J.-C. Micheau, C. Coudret, R. Sanchez, G. Guirado and S. Delbaere, *Chem.–Eur. J.*, 2012, **18**, 6568–6575.
- 12 A. T. Bens, D. Frewert, K. Kodatis, C. Kryschi, H.-D. Martin and H. P. Trommsdorff, *Eur. J. Org. Chem.*, 1998, 2333–2338.
- 13 M. K. Hossain, M. Takeshita and T. Yamato, *Eur. J. Org. Chem.*, 2005, 2771–2776.
- 14 S. Takami, T. Kawai and M. Irie, *Eur. J. Org. Chem.*, 2002, 3796–3800.
- 15 H.-L. Wong, C.-H. Tao, N. Zhu and V. W.-W. Yam, *Inorg. Chem.*, 2011, **50**, 471–481.
- 16 K. Higashiguchi, K. Matsuda, N. Tanifuji and M. Irie, *J. Am. Chem. Soc.*, 2005, **127**, 8922–8923.
- 17 A. E. Keirstead, J. W. Bridgewater, Y. Terazono, G. Kodis, S. Straight, P. A. Liddell, A. L. Moore, T. A. Moore and D. Gust, *J. Am. Chem. Soc.*, 2010, **132**, 6588–6595.
- 18 H. Choi, H. Lee, Y. Kang, E. Kim, S. O. Kang and J. Ko, *J. Org. Chem.*, 2005, **70**, 8291–8297.

- 19 K. Morimitsu, K. Shibata, S. Kobatake and M. Irie, *J. Org. Chem.*, 2002, **67**, 4574–4578.
- 20 A. Osuka, D. Fujikane, H. Shinmori, S. Kobatake and M. Irie, *J. Org. Chem.*, 2001, **66**, 3913–3923.
- 21 J. Cai, A. Farhat, P. B. Tsitovitch, V. Bodani, R. D. Toogood and R. S. Murphy, *J. Photochem. Photobiol., A*, 2010, **212**, 176–182.
- 22 S. Wang, X. Li, S. Cheng, Y. Feng and H. Tian, *Mol. Cryst. Liq. Cryst.*, 2005, **431**, 369–376.
- 23 M. Takeshita, C. Tanaka, T. Miyazaki, Y. Fukushima and M. Nagai, *New J. Chem.*, 2009, **33**, 1433–1438.
- 24 Y. Lin, J. Yuan, M. Hu, J. Cheng, J. Yin, S. Jin and S. H. Liu, *Organometallics*, 2009, **28**, 6402–6409.
- 25 L. Ordroneau, V. Aubert, R. Métivier, E. Ishow, J. Boixel, K. Nakatani, F. Ibersiene, D. Hammoutène, A. Boucekkine, H. L. Bozec and V. Guerschais, *Phys. Chem. Chem. Phys.*, 2012, **14**, 2599–2605.
- 26 H. Choi, I. Jung, K. H. Song, K. Song, D.-S. Shin, S. O. Kang and J. Ko, *Tetrahedron*, 2006, **62**, 9059–9065.
- 27 M. Irie, T. Eriguchi, T. Takada and K. Uchida, *Tetrahedron*, 1997, **53**, 12263–12271.
- 28 I. Jung, H. Choi, E. Kim, C.-H. Lee, S. O. Kang and J. Ko, *Tetrahedron*, 2005, **61**, 12256–12263.
- 29 H. Miyasaka, M. Murakami, A. Itaya, D. Guillaumont, S. Nakamura and M. Irie, *J. Am. Chem. Soc.*, 2001, **123**, 753–754.
- 30 M. Murakami, H. Miyasaka, T. Okada, S. Kobatake and M. Irie, *J. Am. Chem. Soc.*, 2004, **126**, 14764–14772.
- 31 Y. Tsuboi, R. Shimizu, T. Shoji and N. Kitamura, *J. Am. Chem. Soc.*, 2009, **131**, 12623–12627.
- 32 M. T. Indelli, S. Carli, M. Ghirotti, C. Chiorboli, M. Ravaglia, M. Garavelli and F. Scandola, *J. Am. Chem. Soc.*, 2008, **130**, 7286–7299.
- 33 S. Lee, Y. You, K. Ohkubo, S. Fukuzumi and W. Nam, *Org. Lett.*, 2012, **14**, 2238–2241.
- 34 K. Motoyama, T. Koike and M. Akita, *Chem. Commun.*, 2008, 5812–5814.
- 35 Y. Tanaka, T. Ishisaka, A. Inagaki, T. Koike, C. Lapinte and M. Akita, *Chem.–Eur. J.*, 2010, **16**, 4762–4776.
- 36 B. Gorodetsky and N. R. Branda, *Adv. Funct. Mater.*, 2007, **17**, 786–796.
- 37 B. Gorodetsky, H. D. Samachetty, R. L. Donkers, M. S. Workentin and N. R. Branda, *Angew. Chem., Int. Ed.*, 2004, **43**, 2812–2815.
- 38 A. Peters and N. R. Branda, *Chem. Commun.*, 2003, 954–955.
- 39 H. D. Samachetty and N. R. Branda, *Chem. Commun.*, 2005, 2840–2842.
- 40 A. Peters and N. R. Branda, *J. Am. Chem. Soc.*, 2003, **125**, 3404–3405.
- 41 W. R. Browne, J. J. D. de Jong, T. Kudernac, M. Walko, L. N. Lucas, K. Uchida, J. H. van Esch and B. L. Feringa, *Chem.–Eur. J.*, 2005, **11**, 6414–6429.
- 42 W. R. Browne, J. J. D. de Jong, T. Kudernac, M. Walko, L. N. Lucas, K. Uchida, J. H. van Esch and B. L. Feringa, *Chem.–Eur. J.*, 2005, **11**, 6430–6441.
- 43 Y. Moriyama, K. Matsuda, N. Tanifuji, S. Irie and M. Irie, *Org. Lett.*, 2005, **7**, 3315–3318.
- 44 T. Nakashima, Y. Kajiki, S. Fukumoto, M. Taguchi, S. Nagao, S. Hirota and T. Kawai, *J. Am. Chem. Soc.*, 2012, **134**, 19877–19883.
- 45 T. Koshido, T. Kawai and K. Yoshino, *J. Phys. Chem.*, 1995, **99**, 6110–6114.
- 46 G. Guirado, C. Coudret, M. Hliwa and J.-P. Launay, *J. Phys. Chem. B*, 2005, **109**, 17445–17459.
- 47 G. Guirado, C. Coudret and J.-P. Launay, *J. Phys. Chem. C*, 2007, **111**, 2770–2776.
- 48 A. Staykov, J. Areephong, W. R. Browne, B. L. Feringa and K. Yoshizawa, *ACS Nano*, 2011, **5**, 1165–1178.
- 49 S. Lee, Y. You, K. Ohkubo, S. Fukuzumi and W. Nam, *Angew. Chem., Int. Ed.*, 2012, **51**, 13154–13158.
- 50 J. M. R. Narayanam and C. R. J. Stephenson, *Chem. Soc. Rev.*, 2011, **40**, 102–113.
- 51 T. P. Yoon, M. A. Ischay and J. Du, *Nat. Chem.*, 2010, **2**, 527–532.
- 52 C. K. Prier, D. A. Rankic and D. W. C. MacMillan, *Chem. Rev.*, 2013, **113**, 5322–5363.
- 53 D. Ravelli, M. Fagnoni and A. Albin, *Chem. Soc. Rev.*, 2013, **42**, 97–113.
- 54 H. Woo, S. Cho, Y. Han, W.-S. Chae, D.-R. Ahn, Y. You and W. Nam, *J. Am. Chem. Soc.*, 2013, **135**, 4771–4787.
- 55 H. J. Kuhn, S. E. Braslavsky and R. Schmidt, *Pure Appl. Chem.*, 2004, **76**, 2105–2146.
- 56 L. Flamigni, B. Ventura, F. Barigelletti, E. Baranoff, J.-P. Collin and J.-P. Sauvage, *Eur. J. Inorg. Chem.*, 2005, 1312–1318.
- 57 D. Hanss, J. C. Freys, G. Bernardinelli and O. S. Wenger, *Eur. J. Inorg. Chem.*, 2009, 4850–4859.
- 58 C. E. McCusker and F. N. Castellano, *Inorg. Chem.*, 2013, **52**, 8114–8120.
- 59 K.-C. Tang, K. L. Liu and I.-C. Chen, *Chem. Phys. Lett.*, 2004, **386**, 437–441.
- 60 G. J. Hedley, A. Ruseckas and I. D. W. Samuel, *J. Phys. Chem. A*, 2010, **114**, 8961–8968.
- 61 R. A. Marcus, *Angew. Chem., Int. Ed. Engl.*, 1993, **32**, 1111–1121.
- 62 R. A. Marcus and H. Eyring, *Annu. Rev. Phys. Chem.*, 1964, **15**, 155–196.
- 63 D. Rehm and A. Weller, *Ber. Bunsenges. Phys. Chem.*, 1969, **73**, 834–839.
- 64 Y. You, S. Lee, T. Kim, K. Ohkubo, W.-S. Chae, S. Fukuzumi, G.-J. Jhon, W. Nam and S. J. Lippard, *J. Am. Chem. Soc.*, 2011, **133**, 18328–18342.
- 65 M. Murakami, K. Ohkubo and S. Fukuzumi, *Chem.–Eur. J.*, 2010, **16**, 7820–7832.
- 66 R. A. Marcus and N. Sutin, *Biochim. Biophys. Acta, Rev. Bioenerg.*, 1985, **811**, 265–322.
- 67 A. Takai, C. P. Gros, J.-M. Barbe, R. Guilard and S. Fukuzumi, *Chem.–Eur. J.*, 2009, **15**, 3110–3122.
- 68 L. X. Chen, G. Jennings, T. Liu, D. J. Gosztola, J. P. Hessler, D. V. Scaltrito and G. J. Meyer, *J. Am. Chem. Soc.*, 2002, **124**, 10861–10867.
- 69 G. Grampp and G. Hetz, *Ber. Bunsen-Ges. Phys. Chem.*, 1992, **96**, 198–200.
- 70 U. Steiner and G. Winter, *Chem. Phys. Lett.*, 1978, **55**, 364–368.

- 71 T. M. McCleskey, J. R. Winkler and H. B. Gray, *J. Am. Chem. Soc.*, 1992, **114**, 6935–6937.
- 72 M. P. Irvine, R. J. Harrison, G. S. Beddard, P. Leighton and J. K. M. Sanders, *Chem. Phys.*, 1986, **104**, 315–324.
- 73 A. Kapturkiewicz, *Chem. Phys.*, 1992, **166**, 259–273.
- 74 N. Mataga, T. Asahi, Y. Kanda, T. Okada and T. Kakitani, *Chem. Phys.*, 1988, **127**, 249–261.
- 75 P. P. Levin, P. F. Pluzhnikov and V. A. Kuzmin, *Chem. Phys. Lett.*, 1988, **147**, 283–287.
- 76 E. Vauthey, P. Suppan and E. Haselbach, *Helv. Chim. Acta*, 1988, **71**, 93–99.
- 77 P. Chen, R. Duesing, G. Tapolsky and T. J. Meyer, *J. Am. Chem. Soc.*, 1989, **111**, 8305–8306.
- 78 I. R. Gould, D. Ege, S. L. Mattes and S. Farid, *J. Am. Chem. Soc.*, 1987, **109**, 3794–3796.
- 79 I. R. Gould, D. Ege, J. E. Moser and S. Farid, *J. Am. Chem. Soc.*, 1990, **112**, 4290–4301.
- 80 I. R. Gould, J. E. Moser, B. Armitage, S. Farid, J. L. Goodman and M. S. Herman, *J. Am. Chem. Soc.*, 1989, **111**, 1917–1919.
- 81 S. L. Larson, L. F. Cooley, C. M. Elliott and D. F. Kelley, *J. Am. Chem. Soc.*, 1992, **114**, 9504–9509.
- 82 J. R. Miller, J. V. Beitz and R. K. Huddleston, *J. Am. Chem. Soc.*, 1984, **106**, 5057–5068.
- 83 J. R. Miller, L. T. Calcaterra and G. L. Closs, *J. Am. Chem. Soc.*, 1984, **106**, 3047–3049.
- 84 M. R. Wasielewski, M. P. Niemczyk, W. A. Svec and E. B. Pewitt, *J. Am. Chem. Soc.*, 1985, **107**, 1080–1082.
- 85 E. H. Yonemoto, R. L. Riley, Y. I. Kim, S. J. Atherton, R. H. Schmehl and T. E. Mallouk, *J. Am. Chem. Soc.*, 1992, **114**, 8081–8087.
- 86 C. Zou, J. B. Miers, R. M. Ballew, D. D. Dlott and G. B. Schuster, *J. Am. Chem. Soc.*, 1991, **113**, 7823–7825.
- 87 D. Burget, P. Jacques, E. Vauthey, P. Suppan and E. Haselbach, *J. Chem. Soc., Faraday Trans.*, 1994, **90**, 2481–2487.
- 88 I. R. Gould, R. H. Young, R. E. Moody and S. Farid, *J. Phys. Chem.*, 1991, **95**, 2068–2080.
- 89 K. Kikuchi, Y. Takahashi, M. Hoshi, T. Niwa, T. Katagiri and T. Miyashi, *J. Phys. Chem.*, 1991, **95**, 2378–2381.
- 90 T. Ohno, A. Yoshimura, H. Shioyama and N. Mataga, *J. Phys. Chem.*, 1987, **91**, 4365–4370.
- 91 S. S. Jayanthi and P. Ramamurthy, *J. Phys. Chem. A*, 1997, **101**, 2016–2022.
- 92 E. Vauthey, *J. Phys. Chem. A*, 2001, **105**, 340–348.
- 93 T. Kircher and H.-G. Lohmannsroben, *Phys. Chem. Chem. Phys.*, 1999, **1**, 3987–3992.